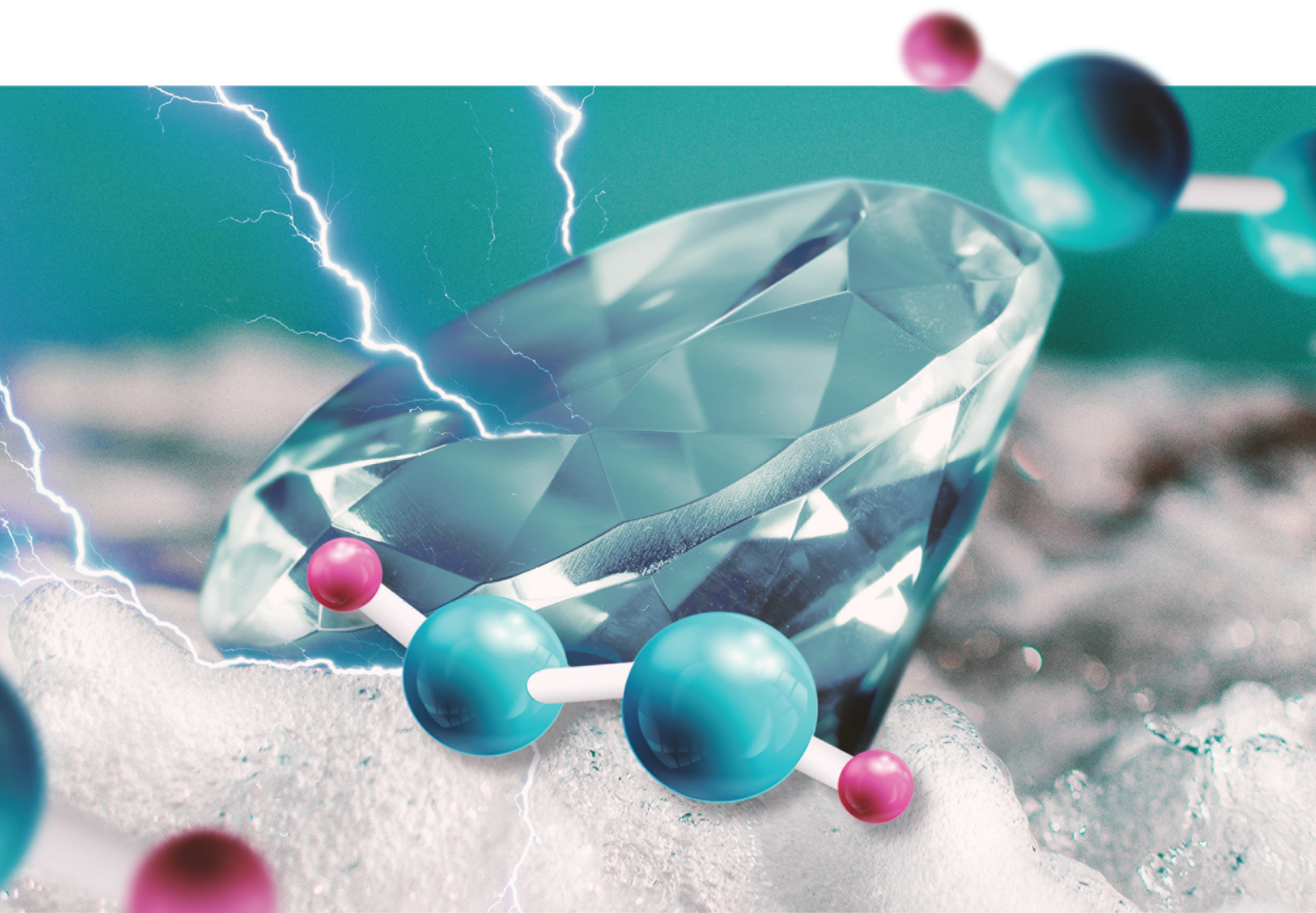


# Green Chemistry

Cutting-edge research for a greener sustainable future

[rsc.li/greenchem](http://rsc.li/greenchem)



ISSN 1463-9262



Cite this: *Green Chem.*, 2022, **24**, 7931

## Anodic generation of hydrogen peroxide in continuous flow<sup>†</sup>

Dhananjai Pangotra, <sup>a,b</sup> Lénárd-István Csepei, <sup>a</sup> Arne Roth, <sup>a</sup> Volker Sieber <sup>a,b</sup> and Luciana Vieira <sup>a\*</sup>

The electrochemical production of hydrogen peroxide ( $\text{H}_2\text{O}_2$ ) is an appealing green alternative to the classic anthraquinone process. Herein, we show the development of a process to produce  $\text{H}_2\text{O}_2$  anodically in continuous flow at high current densities. The role of  $\text{CO}_3^{2-}$  ion activity in enhancing the anodic  $\text{H}_2\text{O}_2$  generation using a commercial boron-doped diamond (BDD) electrode is investigated in detail. The process development comprising the optimization of electrolyte flow type and flow rates enabled electrochemical operation at current densities up to  $700 \text{ mA cm}^{-2}$ , with Faraday efficiencies up to 78%, and the highest-ever reported  $\text{H}_2\text{O}_2$  production rate of  $79 \mu\text{mol min}^{-1} \text{ cm}^{-2}$ . Continuous flow experiments are essential for technical applications, which is one of the first upscaling steps. A continuous and stable  $\text{H}_2\text{O}_2$  productivity with constant production rates for up to 28 hours was achieved. Our experiments unfold the importance of electrochemical process development and the interplay of the electrode, electrolyte, and operating cell parameters to achieve a highly efficient, scalable, stable, and continuous system for the  $2\text{e}^-$  water oxidation to  $\text{H}_2\text{O}_2$ .

Received 11th July 2022,  
Accepted 8th August 2022

DOI: 10.1039/d2gc02575b  
rsc.li/greenchem

## Introduction

Hydrogen peroxide ( $\text{H}_2\text{O}_2$ ) is a widely used chemical with a market evaluated at \$4 billion in 2020, forecasted to grow to \$5.2 billion by 2026.<sup>1</sup> Its strong oxidizing capability enables a broad application in the chemical industry. Moreover, because it releases only water ( $\text{H}_2\text{O}$ ) and oxygen ( $\text{O}_2$ ) as a side-product,  $\text{H}_2\text{O}_2$  is extensively used as a green oxidant. Industrial applications include drinking water<sup>2,3</sup> and wastewater treatment,<sup>4,5</sup> bleaching,<sup>6</sup> desulfurization of conventional energy carriers<sup>7</sup> and bio-based feedstocks,<sup>8,9</sup> sanitation,<sup>10</sup> organic synthesis,<sup>11-13</sup> and aerospace fuels.<sup>14</sup> New niche of applications in catalyst synthesis,<sup>15</sup> biofuel generation,<sup>16</sup> and desulfurization of biogas<sup>17</sup> are also expected to ramp up the demand for  $\text{H}_2\text{O}_2$  in the future. Hence, in the context of these broad application spectra,  $\text{H}_2\text{O}_2$  is among the 100 most essential chemicals globally.<sup>18,19</sup>

The industrial production of  $\text{H}_2\text{O}_2$  is mainly through the anthraquinone autoxidation (AO) process. The AO-process is

considerably energy-demanding (aggregate consumption up to  $17.6 \text{ kW h kg}^{-1} \text{ H}_2\text{O}_2$ ),<sup>20</sup> uses large amounts of organic solvents and involves remarkable risks associated with hydrogenation and oxidation reactions under high  $\text{H}_2/\text{O}_2$  pressure.<sup>21</sup> Furthermore, it requires expensive palladium-based catalysts and complex, large-scale equipment.<sup>22</sup> The industrial AO process involves distillation of  $\text{H}_2\text{O}_2$  to generate large volumes of concentrated solution (from 40 to 70 wt%),<sup>23</sup> which is required for its transportation and very specific applications. Nevertheless, the primary use of  $\text{H}_2\text{O}_2$  in bleaching and disinfectant requires  $\text{H}_2\text{O}_2$  concentrations from 3 to 8 wt%.<sup>24,25</sup> While transportation of  $\text{H}_2\text{O}_2$  in high concentrations is risky, shipping in lower concentrations poses the disadvantage of moving mainly water, thus negatively affecting the carbon footprint and economic viability of the product. Therefore, a portable device for decentralized and on-demand  $\text{H}_2\text{O}_2$  production only based on water, air, and (renewable) electric energy as input provides a desirable local and “green” solution for the supply of  $\text{H}_2\text{O}_2$  where it is needed.

The electrochemical production of  $\text{H}_2\text{O}_2$  is based on water, air, and renewable electric energy as primary feedstocks. Therefore, it is an elegant green solution for onsite and on-demand  $\text{H}_2\text{O}_2$  production, also avoiding risks associated with large-scale storage and transportation of highly concentrated  $\text{H}_2\text{O}_2$  solutions.<sup>22</sup> There are two electrochemical routes for  $\text{H}_2\text{O}_2$  production: the cathodic oxygen reduction reaction (ORR, eqn (1)) and the anodic water oxidation reaction (WOR, eqn (2)). Both pathways involve a two-electron transfer reac-

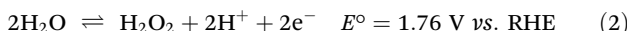
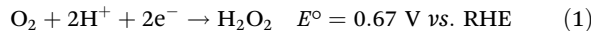
<sup>a</sup>Fraunhofer Institute of Interfacial Engineering and Biotechnology IGB, Bio-, Electro-, and Chemocatalysis BioCat, Straubing Branch, Schulgasse 11a, 94315 Straubing, Germany. E-mail: luciana.vieira@igb.fraunhofer.de

<sup>b</sup>Chair of Chemistry for Biogenic Resources, Campus Straubing for Biotechnology and Sustainability, Technical University of Munich, Schulgasse 16, 94315 Straubing, Germany

† Electronic supplementary information (ESI) available. See DOI: <https://doi.org/10.1039/d2gc02575b>



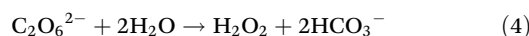
tion.<sup>22</sup> The WOR pathway at the anode is particularly attractive because it can be coupled with cathodic reactions running on large scales, such as the CO<sub>2</sub> reduction reaction (CO<sub>2</sub>RR) and the water electrolysis for hydrogen evolution reaction (HER).<sup>26</sup> Currently, both reactions are coupled with WOR to O<sub>2</sub>, which besides being harmless, is an economically insignificant half-cell reaction and utilizes expensive and critical electrode materials such as iridium.<sup>27,28</sup> Combining anodic and cathodic processes that generate value-added products can enhance the overall cost efficiency of the whole production process.



The electrochemical WOR to H<sub>2</sub>O<sub>2</sub> has gained massive interest in the last years. A strong focus on catalyst development has been crucial for reaction improvement leading to a significant increase in efficiency, selectivity, and stability. Catalysts based on metal oxides such as CaSnO<sub>3</sub>,<sup>29–31</sup> BiVO<sub>4</sub>,<sup>32</sup> and ZnO,<sup>33</sup> as well as on metal porphyrin complexes of Ge<sup>34</sup> and Al<sup>35</sup> have been reported to be highly active catalysts for WOR. Another class of promising materials are boron-doped diamond (BDD) electrodes.<sup>36–38</sup> BDDs are robust electrodes with remarkably high overpotential for oxygen evolution reaction (OER). By suppressing O<sub>2</sub> evolution, high efficiency for H<sub>2</sub>O<sub>2</sub> production is obtained on BDD.<sup>39</sup> Such materials have been used as anode for waste-water treatment for a long time.<sup>40</sup> Recent progress on the properties of BDD materials has significantly enhanced H<sub>2</sub>O<sub>2</sub> production performance, leading to outstanding production rates of 74.6 μmol min<sup>-1</sup> cm<sup>-2</sup> H<sub>2</sub>O<sub>2</sub> and peak faradaic efficiency (FE) of 87%.<sup>38</sup>

Nevertheless, all reports of WOR to H<sub>2</sub>O<sub>2</sub> on BDD have so far been carried out in electrochemical H-cell setups.<sup>37,38</sup> In this context, the process transfer to electrochemical flow cells would be the first step toward technical applications, continuous production and scale-up.<sup>41</sup> Despite the remarkable benefits of electrochemical flow systems in terms of their operational conditions and scalability potential, only a few studies on WOR in flow cells have been reported up to date.<sup>36,42</sup>

Herein, we exploit the remarkable properties of a commercial BDD electrode for the anodic production of H<sub>2</sub>O<sub>2</sub> in a scalable and continuous flow process. Our previous work reported a direct relationship between the ionic activity of CO<sub>3</sub><sup>2-</sup> and enhanced anodic H<sub>2</sub>O<sub>2</sub> production on commercial carbon fiber paper (CFP) anodes.<sup>42</sup> A cyclic mechanism of H<sub>2</sub>O<sub>2</sub> production catalyzed by carbonate ions was proposed through the formation of peroxodicarbonate species (C<sub>2</sub>O<sub>6</sub><sup>2-</sup>) (eqn (3) and (4)).<sup>42</sup>



This mechanism was based on the correlation between the calculated activity of carbonate ions (CO<sub>3</sub><sup>2-</sup>) in the electrolyte and the observed H<sub>2</sub>O<sub>2</sub> formation rate, later confirmed by *in situ* infrared spectroscopy (ATR-FTIR) by Gill *et al.*<sup>43</sup>

In the present study, we extended the scope to show a continuous flow process using a commercial BDD electrode in combination with an optimized carbonate-based electrolyte system. We investigated and compared different flow setups (circular and single-pass) as well as the effect of flow rate on FE and production rate in continuous mode at current densities of up to 700 mA cm<sup>-2</sup>. Our experimental results show the crucial importance of the electrochemical process development beyond catalyst and electrolyte.

## Experimental section

### Materials

Potassium hydrogen carbonate (KHCO<sub>3</sub>, Sigma Aldrich, 99.5%), potassium carbonate (K<sub>2</sub>CO<sub>3</sub>, ReagentPlus®, 99%), titanium(IV) oxysulfate (TiOSO<sub>4</sub>, ≥29% Ti (as TiO<sub>2</sub>) basis, technical), and sodium metasilicate (Na<sub>2</sub>SiO<sub>3</sub>) were purchased from Sigma Aldrich. Potassium hydroxide (KOH, ≥85%) was obtained from Carl Roth. All materials and chemicals were used as received.

### Electrochemical experiments

Electrochemical measurements were performed using an Autolab PGSTAT128N potentiostat/galvanostat equipped with a 10 A booster. A two-compartment H-cell divided by Nafion 117 (Ion Power, Germany) cation exchange membrane (CEM) was used for preliminary studies. The anode was a 5 cm<sup>2</sup> (geometric area) BDD electrode sputtered on a Si substrate and with boron doping between 2000 to 5000 ppm (DIACHEM®, Condias GmbH, Fig. S1, ESI†). The auxiliary cathode was an IrO<sub>2</sub>/Ti mesh, and the reference electrode a Ag/AgCl system in 3.5 mol L<sup>-1</sup> KCl (eDAQ). The gap between cathode and anode was 6 cm. Each compartment of the H-cell was filled with 25 mL of electrolyte. Linear sweep voltammetry (LSV) was recorded at a scan rate of 100 mV s<sup>-1</sup>. Galvanostatic experiments were carried out at current densities ranging from 10 to 300 mA cm<sup>-2</sup> using bicarbonate (HCO<sub>3</sub><sup>-</sup>) and carbonate (CO<sub>3</sub><sup>2-</sup>) electrolytes. Current densities were calculated based on the geometric area of the electrode. Chronopotentiometry measurements were performed under a constant stirring rate of 1000 rpm with a Teflon coated magnetic stirrer. An ice bath was used to avoid thermal decomposition of generated H<sub>2</sub>O<sub>2</sub>. The potentials are reported against the reversible hydrogen electrode (RHE), calculated by the eqn (5).

$$E_{\text{RHE}} = E_{\text{Ag/AgCl}} + 0.059 \text{ pH} + E_{\text{Ag/AgCl}}^\circ \quad E_{\text{Ag/AgCl}}^\circ = 0.205 \text{ V} \quad (5)$$

Experiments under flow were performed using a microflow cell (Electrocell, Denmark) with a unique design from Siemens Energy for the CO2EXIDE project (Horizon 2020, grant agreement no. 768789). The cell was equipped with 10 cm<sup>2</sup> (3 × 3.5 cm) electrodes (cathode and anode) separated by a Nafion 117 membrane. A carbon electrode was used as a cathode, and DIACHEM® BDD/Ta (2000–5000 ppm B doping, Condias GmbH) was used as an anode, with an electrode distance of 8 mm. If not otherwise specified, the anolyte and catholyte

volume were 200 mL for each half-cell. The electrolyte flow was controlled by a flow pump (Watson-Marlow) in a flow range varying from 2 to 120 mL min<sup>-1</sup>. The pH and conductivity of the electrolyte were monitored with a pH-meter (VWR pH 3210) and a conductometer (VWR pHenomenal® CO 3100 H), respectively. All flow experiments were carried out with 2 mol L<sup>-1</sup> K<sub>2</sub>CO<sub>3</sub>. The electrolyte flow setup was varied as circular or single-pass. Circular flow experiments were performed at a constant flow rate of 100 mL min<sup>-1</sup>, with Na<sub>2</sub>SiO<sub>3</sub> as a stabilizer in the electrolyte and regulated at a pH of 12.6. The single-pass flow rate was varied between 5 and 100 mL min<sup>-1</sup>. Moreover, in single-pass flow experiments, the electrolyte containing H<sub>2</sub>O<sub>2</sub> was collected in a separate reservoir. Anolyte samples were collected periodically after having passed the cell and before collecting in the reservoir.

### Quantitative product analysis

The quantification of the anodically generated H<sub>2</sub>O<sub>2</sub> was performed using the TiOSO<sub>4</sub> method as described in the literature.<sup>39,44,45</sup> In short, 0.1 mol L<sup>-1</sup> TiOSO<sub>4</sub> in 2 mol L<sup>-1</sup> H<sub>2</sub>SO<sub>4</sub> solution was prepared prior to the H<sub>2</sub>O<sub>2</sub> detection. 25 µL of anolyte sample was mixed with 975 µL of 0.1 mol L<sup>-1</sup> TiOSO<sub>4</sub> solution in a standard cuvette. In the presence of H<sub>2</sub>O<sub>2</sub>, a color change from colorless to yellow is observed due to the formation of pertitanic acid (eqn (6)). The absorbance of pertitanic acid was measured at 407 nm using a Shimadzu UV-1800 spectrophotometer. The molar extinction coefficient ( $\epsilon_{407\text{nm}}$ ) is  $6.89 \times 10^2$  L mol<sup>-1</sup> cm<sup>-1</sup>.<sup>46</sup>



The faradaic efficiency (FE) was calculated with eqn (7):

$$\text{FE}(\%) = \frac{n_{\text{H}_2\text{O}_2} \times z \times F}{q} \times 100 \quad (7)$$

where  $n_{\text{H}_2\text{O}_2}$  is the number of moles of H<sub>2</sub>O<sub>2</sub> (in mol) produced,  $z$  is the electrons required for water oxidation to H<sub>2</sub>O<sub>2</sub> ( $z = 2$ ),  $F$  is the faradaic constant (96 485 C mol<sup>-1</sup>), and  $q$  is the total charge passed (in Coulombs).

The H<sub>2</sub>O<sub>2</sub> production rate is given by eqn (8):

$$\text{Production rate}(\mu\text{mol min}^{-1} \text{cm}^{-2}) = \frac{\text{H}_2\text{O}_2 \text{ detected}(\mu\text{mol})}{\text{time(min)} \times \text{area of the electrode}(\text{cm}^2)}. \quad (8)$$

The energy consumption was calculated according to eqn (9).

$$\text{EC}(\text{kW h kg}^{-1}) = \frac{U \times z \times F}{M \times \text{FE} \times 3600} \times 100. \quad (9)$$

where  $U$  is the applied cell potential (in V), and  $M$  is the molar mass of H<sub>2</sub>O<sub>2</sub> (in g mol<sup>-1</sup>).

### Calculation of ionic activities for HCO<sub>3</sub><sup>-</sup> and CO<sub>3</sub><sup>2-</sup>

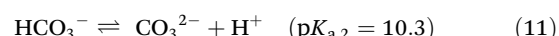
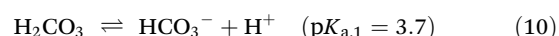
The ionic activity of the bicarbonate ( $a(\text{HCO}_3^-)$ ) and carbonate ( $a(\text{CO}_3^{2-})$ ) ions were calculated as previous reported (eqn (S1)–(S6), ESI†).<sup>42</sup>

## Results and discussion

With the objective of achieving unprecedented levels of performance for the anodic H<sub>2</sub>O<sub>2</sub> generation under technically relevant and scalable operational conditions, this study is divided into two parts: (i) a preliminary evaluation of the electrolyte in an H-cell configuration and (ii) an electrochemical process optimization in a continuous flow reactor. In the first part, the effect of the electrolyte composition on WOR to H<sub>2</sub>O<sub>2</sub> is qualitatively and quantitatively evaluated. In the second part, the process is transferred to a continuous flow reactor under optimized electrolyte conditions, where the effect of flow setup and flow rate is investigated and optimized towards higher anodic H<sub>2</sub>O<sub>2</sub> productivity.

### The electrolyte effect

Bicarbonate solutions have been widely used for WOR to H<sub>2</sub>O<sub>2</sub>.<sup>37,43,47</sup> The molar fraction of the bicarbonate (HCO<sub>3</sub><sup>-</sup>)/carbonate (CO<sub>3</sub><sup>2-</sup>) species in solution is dependent on the pH of the electrolyte (eqn (10) and (11)).



Basic pHs favor higher activity of carbonate ions, which promotes the WOR to H<sub>2</sub>O<sub>2</sub> through the intermediate formation of peroxodicarbonate species (C<sub>2</sub>O<sub>6</sub><sup>2-</sup>, Scheme S1, ESI†).<sup>42,43</sup> Although the benefits of high pH are significant, it can be detrimental due to the low stability of H<sub>2</sub>O<sub>2</sub> under alkaline conditions. Therefore, a chemical stabilizer was added to the anolyte to decelerate the alkaline decomposition of H<sub>2</sub>O<sub>2</sub>.<sup>42</sup>

WOR in 2 mol L<sup>-1</sup> solutions of bicarbonate (KHCO<sub>3</sub>, at pH 8.4) and carbonate (K<sub>2</sub>CO<sub>3</sub>, at pH 12.6) electrolytes were evaluated by linear sweep voltammetry (LSV) on BDD electrodes (Fig. 1a). The two electrolytes show a distinct current density profile. At +3.2 V vs. RHE, the current density is substantially higher for K<sub>2</sub>CO<sub>3</sub> (155 mA cm<sup>-2</sup>) compared to KHCO<sub>3</sub> (140 mA cm<sup>-2</sup>). The onset potential, defined as the potential where the current density starts to increase exponentially, is also considerably lower for carbonate (+2.45 V vs. RHE) than for bicarbonate solutions (+2.66 V vs. RHE). Both aspects, higher current density and low onset potential, indicate a higher electrochemical activity for WOR in K<sub>2</sub>CO<sub>3</sub> electrolytes compared to KHCO<sub>3</sub>.

The effect of current density on H<sub>2</sub>O<sub>2</sub> production for these two carbonate-based electrolytes (HCO<sub>3</sub><sup>-</sup> and CO<sub>3</sub><sup>2-</sup>) was further evaluated by chronopotentiometry (CP) at pH 8.4 and pH 12.6 (Fig. 1b). Increasing the current density results in a higher H<sub>2</sub>O<sub>2</sub> concentration for both electrolytes, yet carbonate-based electrolytes lead to higher overall H<sub>2</sub>O<sub>2</sub> concentrations.<sup>38,42,48</sup> A maximum of 70 mmol L<sup>-1</sup> of H<sub>2</sub>O<sub>2</sub> was obtained in carbonate at 300 mA cm<sup>-2</sup>, compared to only 16.4 mmol L<sup>-1</sup> H<sub>2</sub>O<sub>2</sub> in bicarbonate.

The FE at applied different current densities showed a peak of 57% in carbonate solutions at 100 mA cm<sup>-2</sup>, whereas the



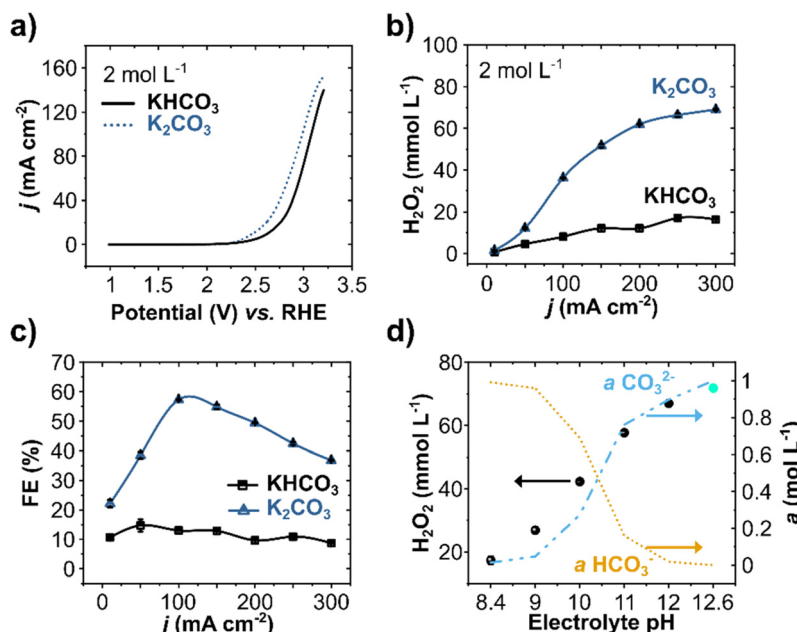


**Fig. 1** WOR to  $\text{H}_2\text{O}_2$  in  $2 \text{ mol L}^{-1}$   $\text{KHCO}_3$  and  $\text{K}_2\text{CO}_3$  electrolytes. (a) Anodic LSV starting from  $+0.18 \text{ V}$  vs.  $\text{Ag}/\text{AgCl}$  (calculated vs. RHE) with a scan rate of  $100 \text{ mV s}^{-1}$ . (b)  $\text{H}_2\text{O}_2$  concentration and (c) FE at the indicated applied current densities for 10 minutes at each step. (d) Galvanostatic polarization at  $300 \text{ mA cm}^{-2}$  for 10 minutes in  $2 \text{ mol L}^{-1}$   $\text{KHCO}_3$  (at adjusted pH values from 8.4 to 12) and  $2 \text{ mol L}^{-1}$   $\text{K}_2\text{CO}_3$  (pH 12.6) and the corresponding calculated ionic activity for  $\text{HCO}_3^-$  and  $\text{CO}_3^{2-}$  ions. The experiments were performed using a  $5 \text{ cm}^2$  BDD anode in a two-compartment H-cell cooled in an ice bath. The electrolyte was changed between the galvanostatic steps and kept under constant stirring of  $1000 \text{ rpm}$ .

FEs in bicarbonate electrolytes lay between 10 and 15% for all current densities (Fig. 1c). Higher FE for carbonate solutions (at least four times higher than in bicarbonate) confirms that higher pH regimes enhance the electrochemical production of  $\text{H}_2\text{O}_2$  on BDD anodes, consistent with our previous studies with carbon anodes.<sup>42</sup> At current densities higher than  $100 \text{ mA cm}^{-2}$ , the FE decreases, reaching 36% at  $300 \text{ mA cm}^{-2}$ , where the highest  $\text{H}_2\text{O}_2$  concentration was achieved. This lower FE, despite higher net  $\text{H}_2\text{O}_2$  concentrations, indicates a combined effect of enhanced oxygen evolution and electrolytic  $\text{H}_2\text{O}_2$  decomposition.<sup>37</sup> Notwithstanding, anodic  $\text{H}_2\text{O}_2$  formation reached a partial current density ( $j_{\text{H}_2\text{O}_2}$ ) of  $110 \text{ mA cm}^{-2}$  and a production rate of  $35 \mu\text{mol min}^{-1} \text{ cm}^{-2}$  at  $300 \text{ mA cm}^{-2}$  (Fig. S3, ESI†).

As different carbonate species ( $\text{H}_2\text{CO}_3$ ,  $\text{HCO}_3^-$ , and  $\text{CO}_3^{2-}$ ) can be formed by varying the pH of the solution, the ionic activity for  $\text{HCO}_3^-$  ( $a(\text{HCO}_3^-)$ ) and  $\text{CO}_3^{2-}$  ( $a(\text{CO}_3^{2-})$ ) species in the electrolyte was calculated as a function of pH for the range of pH 8.4 to 12.6 (Fig. 1d). In the same pH range, the anodic  $\text{H}_2\text{O}_2$  production at  $300 \text{ mA cm}^{-2}$  was evaluated experimentally. The pH of the  $2 \text{ mol L}^{-1}$   $\text{KHCO}_3$  was adjusted using KOH salt. The calculated activity profile for  $a(\text{HCO}_3^-)$  and  $a(\text{CO}_3^{2-})$  show a remarkable correlation with the experimentally measured anodic  $\text{H}_2\text{O}_2$  production. Higher  $a(\text{CO}_3^{2-})$  at higher pH values lead to significantly higher  $\text{H}_2\text{O}_2$  concentrations. A considerable visual difference in the anode was also observed at higher pH values, as the  $\text{O}_2$  evolution substantially decreased. Higher  $\text{H}_2\text{O}_2$  production at higher pH is consistent with our proposed mechanism, which involves the oxidation of

carbonate ions to peroxodicarbonate species as intermediates.<sup>42</sup>

### WOR in a continuous flow reactor

Envisioning the scale-up and technical application of anodic water oxidation to  $\text{H}_2\text{O}_2$ , a flow cell setup was used for further investigations. The electrochemical flow mode/setup (circular or single-pass), the electrolyte flow rate, and the long-term stability of the system were investigated and optimized.

### Anodic $\text{H}_2\text{O}_2$ production in circular flow

Circular flow experiments allow the increase of product concentration in the electrolyte reservoir by recirculating it through the cell multiple times (Fig. 2a and Fig. S4, ESI†). Galvanostatic experiments on circular flow were carried out at current densities of 100, 200, and  $300 \text{ mA cm}^{-2}$  (Fig. 2b) with a constant flow rate of  $100 \text{ mL min}^{-1}$ . The highest  $\text{H}_2\text{O}_2$  concentration was obtained at  $200 \text{ mA cm}^{-2}$  ( $58 \text{ mmol L}^{-1}$ ) after recirculating for 150 minutes. In all experiments, the FE reached its maximum peak at 15 minutes, and longer reaction times resulted in lower FE and formation rates (Fig. 2c and Fig. S5a, ESI†), indicating not only WOR to  $\text{O}_2$  as also the electrochemical decomposition of  $\text{H}_2\text{O}_2$ . Such production rate decrease with time was also observed in H-cell experiments (Fig. S6, ESI†), and it is consistent with the literature.<sup>37,42,49</sup>

The specific electric energy consumption for the anodic  $\text{H}_2\text{O}_2$  generation was calculated for the first reaction stage of high formation rate (first 15 minutes, Fig. 2d) and for the



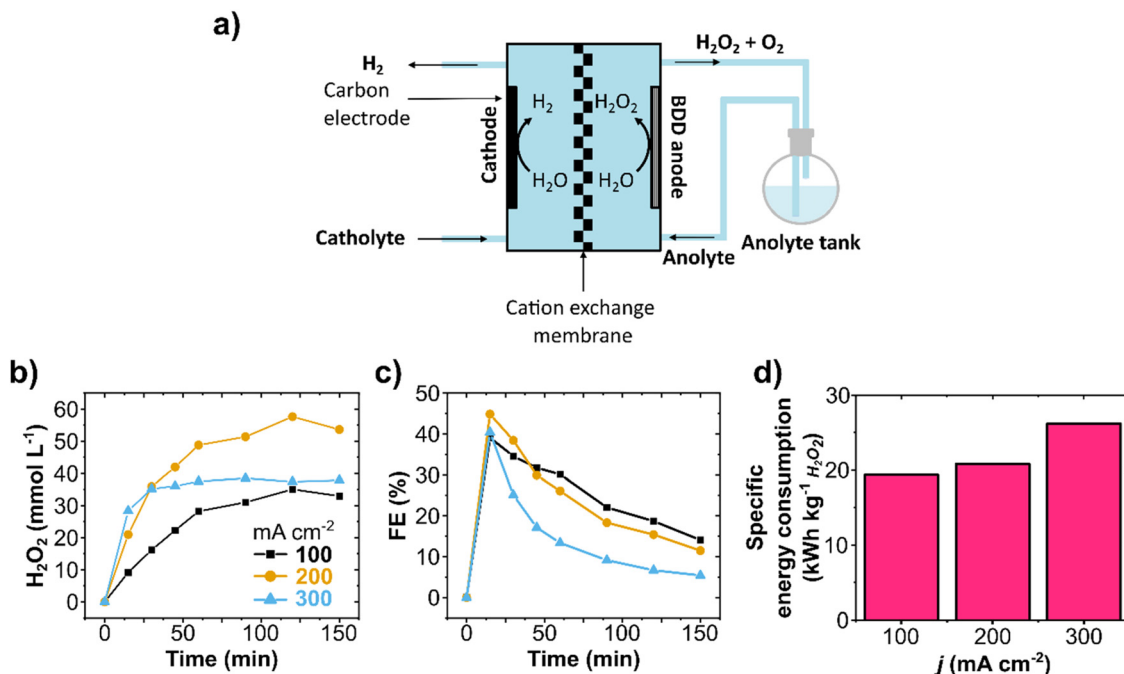


**Fig. 2** Anodic H<sub>2</sub>O<sub>2</sub> production in a circular flow reactor. (a) Schematic representation of the flow cell with circular flow. (b) H<sub>2</sub>O<sub>2</sub> concentration and (c) FE obtained at different applied current densities. (d) Energy consumption to produce 1 kg of H<sub>2</sub>O<sub>2</sub> based on the peak FE (at 15 min) at each applied current density. The flow cell was equipped with a carbon cathode and a BDD/Ta anode (both with a 10 cm<sup>2</sup> geometric area) separated by a Nafion 117 membrane. Each cell compartment contained a reservoir with 200 mL of 2 mol L<sup>-1</sup> K<sub>2</sub>CO<sub>3</sub> electrolyte circulating at 100 mL min<sup>-1</sup> flow rate. 90 mmol L<sup>-1</sup> Na<sub>2</sub>SiO<sub>3</sub> was added to the anolyte as a chemical stabilizer to avoid H<sub>2</sub>O<sub>2</sub> decomposition. The pH of the anolyte was kept constant at 12.6.

whole reaction time (150 minutes, Fig. S5c and Table S1, ESI<sup>†</sup>). The specific energy consumption of a product is one of the most basic approaches to determining the unit energy consumption.<sup>50</sup> The first reaction stage at 100 mA cm<sup>-2</sup> had a specific energy consumption of 19.3 kW h kg<sup>-1</sup>, which raised considerably to 26 kW h kg<sup>-1</sup> at 300 mA cm<sup>-2</sup>. After 150 minutes of reaction with recirculation (75 cycles), the specific energy consumption was as high as 196 kW h kg<sup>-1</sup> at 300 mA cm<sup>-2</sup> (Fig. S5c and Table S1, ESI<sup>†</sup>). At a flow rate of 100 mL min<sup>-1</sup> and 200 mL anolyte volume, each recirculation cycle takes 2 minutes. The increase in energy consumption after 15 minutes is mainly due to the electrochemical H<sub>2</sub>O<sub>2</sub> decomposition at the electrode surface, which can be particularly prominent at higher current densities (as observed at 300 mA cm<sup>-2</sup>). It is important to notice that the aggregate energy consumption for classical anthraquinone process is in about 17.6 kW h kg<sup>-1</sup> H<sub>2</sub>O<sub>2</sub>.<sup>20</sup> Hence, energy efficiency needs to be improved further for WOR-based H<sub>2</sub>O<sub>2</sub> production. Therefore, a compromise in process parameters (current density, cell potential, cell design, membrane resistivity, *etc.*) should be found.

The effect of recirculating the electrolyte on the anodic generation and electrode decomposition of H<sub>2</sub>O<sub>2</sub> was investigated stepwise by decreasing the electrolyte flow rate from 100 to 10 mL min<sup>-1</sup> and limiting the recirculating steps to four (Fig. 3). Each cycle lasted for 20 minutes, thereafter the electrolyte was recirculated for a new pass cycle. An increase in H<sub>2</sub>O<sub>2</sub>

concentration was observed with each consecutive cycle at 100 and 300 mA cm<sup>-2</sup>, albeit FE and production rate decreased. The H<sub>2</sub>O<sub>2</sub> concentration in the anolyte reached 46 and 110 mmol L<sup>-1</sup> after four cycles at 100 and 300 mA cm<sup>-2</sup>, respectively (Fig. 3a). However, the FE decreased from 40% to 33% (1<sup>st</sup> to 4<sup>th</sup> cycle) at 100 mA cm<sup>-2</sup> and from 45% (1<sup>st</sup> cycle) to 6% during the 4<sup>th</sup> cycle at 300 mA cm<sup>-2</sup> (Fig. 3b). A drastic decrease in production rate (Fig. 3c) from 41 to 7 μmol min<sup>-1</sup> cm<sup>-2</sup> (70% decrease) at 300 mA cm<sup>-2</sup> in comparison to only 12% decrease at 100 mA cm<sup>-2</sup> was observed. The decrease in FE and formation rate with cycle is an effect of the decomposition of electrochemically produced H<sub>2</sub>O<sub>2</sub> on the electrode surface after recirculation, particularly at high current densities, as also observed in continuous circular flow experiments. Additionally, the pH of the electrolyte also decreased with each cycle (Fig. 3d) due to the constant oxidation of OH<sup>-</sup> ions to O<sub>2</sub>. This pH decrease was more pronounced for higher current densities. Thus, the remarkable decline in production rate observed at 300 mA cm<sup>-2</sup> can also be due to the drop in pH, as it plays a direct role in the  $\alpha(\text{CO}_3^{2-})$ , consequently, in the peroxodicarbonate formation and H<sub>2</sub>O<sub>2</sub>.<sup>42</sup> A considerable drop in the electrolyte conductivity was observed at a high current density (Fig. S7a, ESI<sup>†</sup>). The cell potential remained, nevertheless, essentially constant during all four cycles (Fig. S7b, ESI<sup>†</sup>). Increasing the number of cycles increases the overall product concentration, however it has the drawback of decreasing the production rate, and consequently increasing

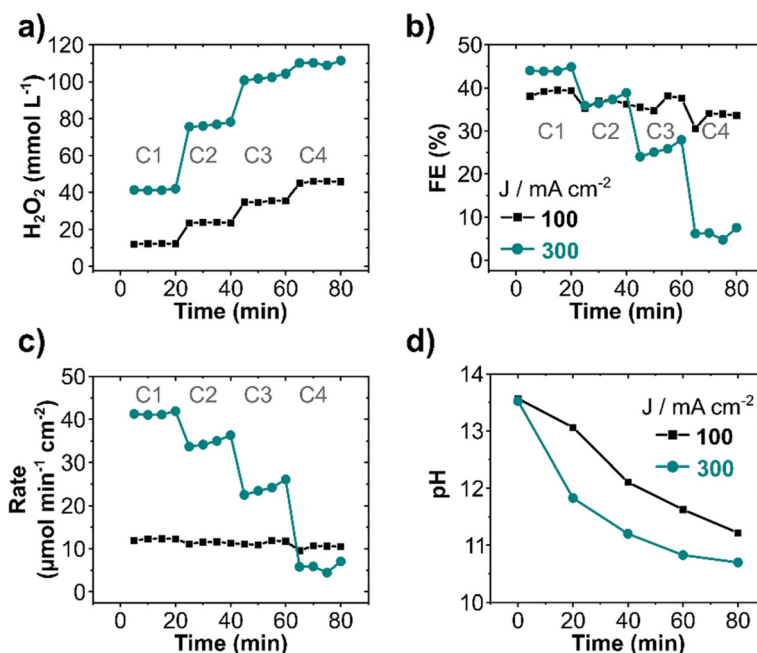


**Fig. 3**  $\text{H}_2\text{O}_2$  generation under electrolyte flow with multiple recirculation cycles. (a) Anodic  $\text{H}_2\text{O}_2$  concentration, (b) FE, (c) production rate, and (d) pH change. The experiments were carried out in a flow cell equipped with  $10 \text{ cm}^2$  BDD as anode and recirculated with  $2 \text{ mol L}^{-1} \text{K}_2\text{CO}_3$  containing  $90 \text{ mmol L}^{-1} \text{Na}_2\text{SiO}_3$  at  $10 \text{ mL min}^{-1}$  flow rate. The total volume of the electrolyte was  $200 \text{ mL}$ . Experiments were performed in 4 cycles of electrolyte flow (indicated as C1 to C4) of 20 minutes each.

the specific energy consumption for  $\text{H}_2\text{O}_2$  production (Fig. S7c, ESI†).

Chemical stabilizers can slightly decrease the decomposition of  $\text{H}_2\text{O}_2$  in the electrolyte. Sodium silicate ( $\text{Na}_2\text{SiO}_3$ ) is a particularly attractive stabilizer because it is not redox-active, thus it does not affect the electrode reactions.<sup>36,42</sup> Circular flow experiments using anolyte with and without  $\text{Na}_2\text{SiO}_3$  revealed that the silicate stabilizer considerably enhances  $\text{H}_2\text{O}_2$  stability upon recirculation (Fig. S8, ESI†). Nevertheless, the challenge of anodic  $\text{H}_2\text{O}_2$  decomposition can be tackled by regularly replacing the electrolyte in batches or optimizing the flow rate for maximum and continuous  $\text{H}_2\text{O}_2$  productivity without recirculation (single-pass flow).

#### Single-pass flow

A single-pass flow mode was employed to minimize performance losses through electrochemical decomposition upon anolyte recirculation (Fig. 4a and Fig. S9, ESI†). In this setup, the anolyte containing the electrochemically generated  $\text{H}_2\text{O}_2$  is not recirculated but optimized for maximum continuous production.

Electrolytic steps of 20 minutes at  $10 \text{ mL min}^{-1}$  electrolyte flow rate were carried out at current densities ranging from  $100$  to  $700 \text{ mA cm}^{-2}$ . The concentration of anodically generated  $\text{H}_2\text{O}_2$  was directly proportional to the current density (Fig. 4b). Starting at  $12 \text{ mmol L}^{-1}$  at  $100 \text{ mA cm}^{-2}$ , a maximum of  $79 \text{ mmol L}^{-1}$   $\text{H}_2\text{O}_2$  was obtained at  $700 \text{ mA cm}^{-2}$ . The  $\text{H}_2\text{O}_2$  production rate was stable and constant during the 20 minutes step, and a maximum of  $79 \mu\text{mol min}^{-1} \text{cm}^{-2}$  was obtained at

$700 \text{ mA cm}^{-2}$  (Fig. S10b and c, ESI†). To the best of our knowledge, this is the highest production rate for the anodic  $\text{H}_2\text{O}_2$  generation so far reported. A detailed literature comparison of production rates is shown in Table S2, ESI†. The partial current density to produce  $\text{H}_2\text{O}_2$  ( $j_{\text{H}_2\text{O}_2}$ ) reached  $250 \text{ mA cm}^{-2}$  (Fig. S10d, ESI†). It is important to remark that this single-pass setup allowed reaching considerably higher current densities, up to  $700 \text{ mA cm}^{-2}$ . In this regard, techno-economic studies show that the economic (cost-related) performance of anodic  $\text{H}_2\text{O}_2$  generation can be enhanced by increasing the current density.<sup>39,51</sup>

A maximum FE of  $50\%$  was achieved at  $300 \text{ mA cm}^{-2}$  (Fig. 4b), which dropped to  $35\%$  at  $700 \text{ mA cm}^{-2}$ . This FE decreases upon increasing current density is likely due to an increase in  $\text{O}_2$  evolution. Although the cell potential increased at higher current densities (from  $4.7 \text{ V}$  at  $100 \text{ mA cm}^{-2}$  to  $9 \text{ V}$  at  $700 \text{ mA cm}^{-2}$ , Fig. S11, ESI†), the total cell potential is still below the maximum recommended ( $11 \text{ V}$ ) to enable the technical feasibility of the setup in combination with HER.<sup>39</sup>

The specific energy consumption was around  $20 \text{ kW h kg}^{-1}$  for current densities up to  $300 \text{ mA cm}^{-2}$  (Fig. 4c). However, the energy consumption takes a steady steep at higher current densities, increasing to  $40 \text{ kW h kg}^{-1}$  at  $700 \text{ mA cm}^{-2}$ , as a considerable share of energy consumption is used for  $\text{O}_2$  production.<sup>42</sup> Since the highest FE and relatively low specific energy consumption were obtained at  $300 \text{ mA cm}^{-2}$ , further optimizations with the single-pass flow were performed at this current density.



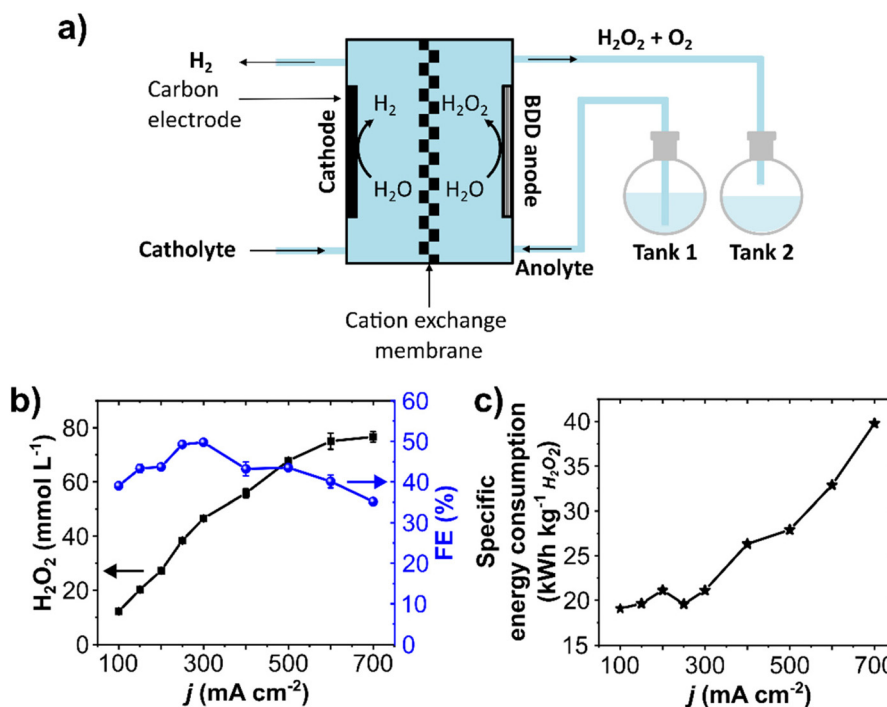


**Fig. 4** Anodic H<sub>2</sub>O<sub>2</sub> production in a single-pass mode flow reactor. (a) Schematic representation of the flow cell with a single-pass flow setup. (b) Average H<sub>2</sub>O<sub>2</sub> concentration, FE, and (c) specific energy consumption at different current densities (20 minutes steps). 200 mL of 2 mol L<sup>-1</sup> K<sub>2</sub>CO<sub>3</sub> + 90 mmol L<sup>-1</sup> Na<sub>2</sub>SiO<sub>3</sub> was used as an anolyte at a 10 mL min<sup>-1</sup> flow rate without recirculation. The flow cell was equipped with a BDD/Ta working electrode (10 cm<sup>2</sup> geometric area) and a carbon cathode.

### Effect of stabilizers at single-pass flow

A chemical stabilizer is essential to avoid chemical and electrochemical decomposition of H<sub>2</sub>O<sub>2</sub>, particularly in a circular flow setup, as observed in our experiments with and without Na<sub>2</sub>SiO<sub>3</sub>, where higher H<sub>2</sub>O<sub>2</sub> concentrations were obtained in the presence of the silicate (Fig. S8, ESI†).<sup>42</sup> However, in a single-pass flow mode, the electrochemical H<sub>2</sub>O<sub>2</sub> decomposition can be minimized by optimizing the residence time of the electrolyte in contact with the electrode surface. Hence, a stabilizer may no longer be necessary.

To validate this hypothesis and to elucidate the effect of chemically stabilizing agents in a single-pass flow system, experiments at 300 mA cm<sup>-2</sup> were carried out with and without a stabilizer. In a single-pass mode, a similar H<sub>2</sub>O<sub>2</sub> concentration of 52 mmol L<sup>-1</sup> was obtained, independently of the presence of Na<sub>2</sub>SiO<sub>3</sub>. However, when the electrochemically produced H<sub>2</sub>O<sub>2</sub> was stored for 3 hours without any applied current, the H<sub>2</sub>O<sub>2</sub> concentration decreased by 42% (from 52 to 29 mmol L<sup>-1</sup>) in the absence of the stabilizer, compared to only 8% (53 to 49 mmol L<sup>-1</sup>) in its presence (Fig. 5). Thus, the use of Na<sub>2</sub>SiO<sub>3</sub> as a stabilizer in single-pass mode does not necessarily enhance the electrochemical H<sub>2</sub>O<sub>2</sub> formation, it rather inhibits the chemical decomposition of H<sub>2</sub>O<sub>2</sub> during storage and thereby increases its bench life. Hence, immediate use of H<sub>2</sub>O<sub>2</sub> in on-site applications can abstain from chemical stabilizers, which could consequently influence the total process costs. In cases requiring intermediate storage of the

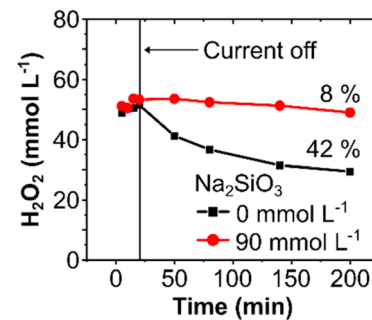


**Fig. 5** Effect of stabilizer on the stability of electrochemically produced H<sub>2</sub>O<sub>2</sub>. Change in H<sub>2</sub>O<sub>2</sub> concentration during electrolyte storage in the absence (■) and presence (●) of 90 mmol L<sup>-1</sup> Na<sub>2</sub>SiO<sub>3</sub> in 2 mol L<sup>-1</sup> K<sub>2</sub>CO<sub>3</sub>. The H<sub>2</sub>O<sub>2</sub> was anodically generated for 20 minutes at 300 mA cm<sup>-2</sup>. Thereafter, electrolyte samples were taken at 30, 60, 120, and 180 minutes from the storage reservoir.

generated H<sub>2</sub>O<sub>2</sub>, however, stabilizers are recommended to avoid substantial chemical losses.

### Effect of flow rate

The flow rate optimization maximizes the transient electrolyte time in the electrochemical cell and, consequently, the continuous anodic H<sub>2</sub>O<sub>2</sub> production in single-pass flow. The experiments described to this point had a constant flow rate of 10 mL min<sup>-1</sup>. Variation of the flow-rate in the range of 5 to

100  $\text{mL min}^{-1}$  in single-pass flow at a constant current density of 300  $\text{mA cm}^{-2}$  shows contrasting shapes for  $\text{H}_2\text{O}_2$  concentrations and FE at different flow rates (Fig. 6a). Slower flow rates (5  $\text{mL min}^{-1}$ ) lead to higher  $\text{H}_2\text{O}_2$  concentrations (75  $\text{mmol L}^{-1}$ ), however, to lower FE (40%). Speeding the flow rate decreases the residence time of a specific electrolyte volume in the vicinity of the electrode, thus minimizing relevant side-reactions, such as  $\text{O}_2$  evolution and electrode decomposition of  $\text{H}_2\text{O}_2$ , and resulting in higher FE and production rate (Fig. 6b). Nevertheless, higher flow rates also decrease the  $\text{H}_2\text{O}_2$  concentration and increase the required electrolyte volume per time, which can be costly. Therefore, a compromise between  $\text{H}_2\text{O}_2$  concentration and FE must be considered depending on the application of anodic  $\text{H}_2\text{O}_2$  production in continuous flow.

Moreover, the corresponding specific energy consumption decreased by around 50% (from 25  $\text{kW h kg}^{-1}$  to 13  $\text{kW h kg}^{-1}$ ) upon increasing the flow rate from 5 to 100  $\text{mL min}^{-1}$  (Fig. 6b). Considering the cost of renewable electricity of 3 cents(\$) per kW per h,<sup>36,52</sup> the specific electricity-related cost of anodic  $\text{H}_2\text{O}_2$  generation (\$ per kg  $\text{H}_2\text{O}_2$ ) at 300  $\text{mA cm}^{-2}$  is

estimated at \$0.77 per kg at 5  $\text{mL min}^{-1}$  and \$0.4 per kg at 100  $\text{mL min}^{-1}$  (Fig. S12, ESI†). Commercial  $\text{H}_2\text{O}_2$  from the anthraquinone process is currently priced at \$1.50 per kg without transportation costs.<sup>36</sup> Nonetheless, it should be noted that our figures for calculated specific energy consumption only include the electric energy required for electrochemical cell operation. Hence, the estimated electricity cost reported in this study is specific to this lab-scale electrochemical cell. Certainly, other operating costs (e.g., material consumption, cell design, cathode material, membrane type, and downstream processing) could and will substantially contribute to the overall cost structure of  $\text{H}_2\text{O}_2$  production *via* WOR. Yet, the cost of electricity to produce  $\text{H}_2\text{O}_2$  at the anode can be further reduced by combining it with an optimized cathodic half-cell reaction such as HER,  $\text{CO}_2\text{RR}$ , or ORR to replace the current WOR to  $\text{O}_2$ .

Finally, a long-term stability study using the optimized single-pass flow setup was performed to produce  $\text{H}_2\text{O}_2$  continuously. The stability of the electrochemical system is essential for its technical application, as it reduces the occurrence of component failures and the associated need to disassemble

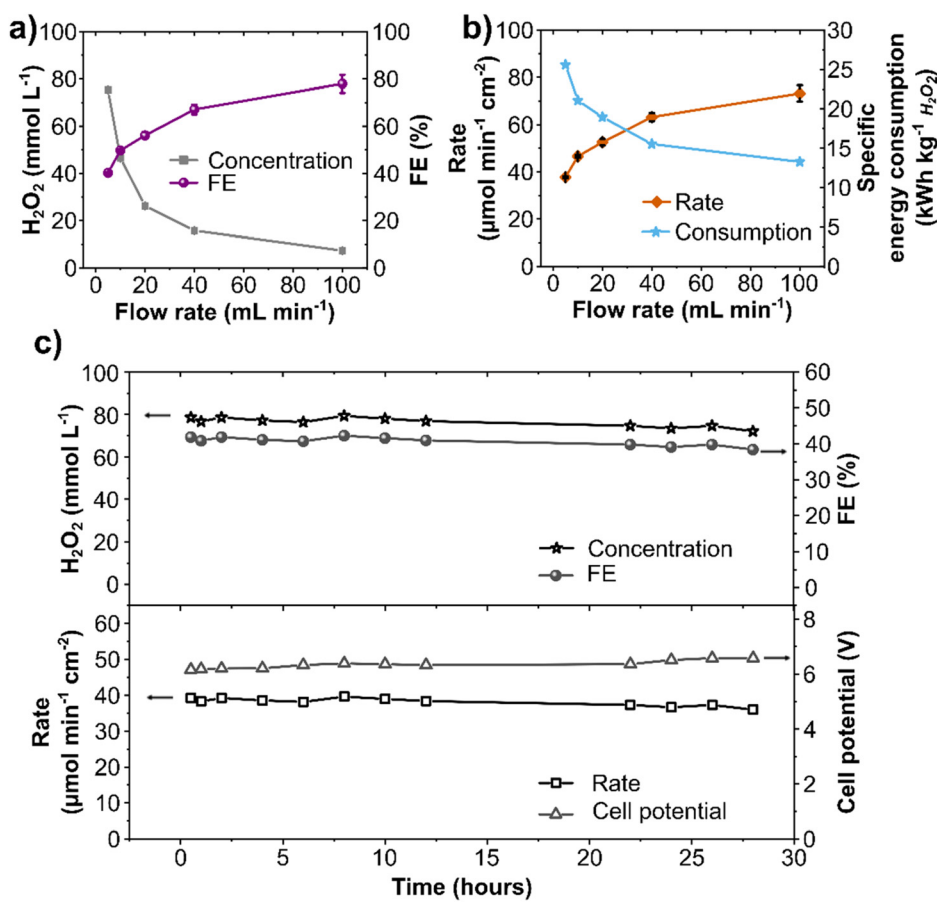


Fig. 6 Flow rate effect on the continuous anodic  $\text{H}_2\text{O}_2$  generation. (a) Anodic  $\text{H}_2\text{O}_2$  concentration and FE, (b) production rate and specific energy consumption to produce 1 kg  $\text{H}_2\text{O}_2$  at different electrolyte flow rates. Experimental conditions: single-pass flow of 200  $\text{mL}$  anolyte ( $2 \text{ mol L}^{-1} \text{K}_2\text{CO}_3$ ) at a constant current density of 300  $\text{mA cm}^{-2}$ . The same electrolyte volume was used for each flow rate, resulting in different durations of the individual experiments. (c) Electrode stability test in a continuous flow setup:  $\text{H}_2\text{O}_2$  concentration, FE, production rate, and cell potential at a  $10 \text{ cm}^2$  BDD at a constant current density of 300  $\text{mA cm}^{-2}$  with a single-pass flow mode of  $2 \text{ mol L}^{-1} \text{K}_2\text{CO}_3$  electrolyte at a flow rate of 5  $\text{mL min}^{-1}$ .



and reassemble the reactor.<sup>53</sup> Galvanostatic experiment at 300 mA cm<sup>-2</sup> was performed in 2 mol L<sup>-1</sup> K<sub>2</sub>CO<sub>3</sub> at a 5 mL min<sup>-1</sup> flow rate for 28 hours (Fig. 6c). Anolyte samples were taken directly from the electrochemical cell outlet, showing a continuous generation of H<sub>2</sub>O<sub>2</sub> for 28 hours with a constant concentration of about 80 mmol L<sup>-1</sup> and a constant FE of 40%. An average production rate of 40 µmol min<sup>-1</sup> cm<sup>-2</sup> was observed with a stable cell potential of 6.3 V throughout the experiment. This stability experiment highlights the effectiveness of an optimized electrochemical setup. Previous reports on electrode stability for WOR to H<sub>2</sub>O<sub>2</sub> using carbonaceous electrodes are restricted to batch mode (H-cells) with low electrolyte volume and at current densities from 100 to 200 mA cm<sup>-2</sup> with a maximum time of 10 hours.<sup>31,36,38</sup> Our last study using commercial carbon fiber paper electrodes reported stable operation for up to 17.5 hours at 100 mA cm<sup>-2</sup>.<sup>42</sup> Herein, we expanded the potential of process development for WOR to H<sub>2</sub>O<sub>2</sub> to reach considerably higher current densities and continuous stable production at a robust commercial BDD electrode. This is also the first comprehensive study of an electrochemical flow system for WOR to H<sub>2</sub>O<sub>2</sub>, which remains stable for 28 hours. Such investigations are essential for future technical electrochemical applications. Moreover, considering that BDD anodes are already used in several electrochemical industrial processes with a lifetime up to several months,<sup>54</sup> it can be expected that H<sub>2</sub>O<sub>2</sub> generation through WOR at BDD anodes can also be operated with high stability and performance for a considerably longer time. Electrode and process stability is an important step forward in terms of scale-up and utilization.

## Conclusions

This research work demonstrates that beyond the catalyst development, the process parameters (including electrolyte type, pH, flow type, and flow rate) can dramatically affect the efficiency of anodic H<sub>2</sub>O<sub>2</sub> production and, consequently, the technical process implementation. The continuous flow process has been developed with commercially available and scalable BDD anodes. Hence, it highlights a robust, stable, and promising foundation for piloting. Future work includes the combination of the anodic H<sub>2</sub>O<sub>2</sub> production with value-added cathodic reactions, with the objective of utilizing the invested redox equivalents most efficiently by exploiting both half-cells. Considering the still high capital expenses for BDD electrodes, other low-cost carbon-based materials are a promising area for further exploration in searching for efficient and scalable WOR to H<sub>2</sub>O<sub>2</sub>. In this context, such research should be performed with a clear perspective of future industrial applications, focusing on relevant and scalable process configurations, as well as resource efficiency, investment, operational cost, and operational stability.

The electrochemical H<sub>2</sub>O<sub>2</sub> production is nonetheless not a replacement for the current industrial AO process. From the perspective of mobile electrochemical prototypes, this is rather

an expansion of the H<sub>2</sub>O<sub>2</sub> market to accommodate decentralized solutions, especially in remote areas where transportation of H<sub>2</sub>O<sub>2</sub> is difficult. As an additional benefit, the anodic H<sub>2</sub>O<sub>2</sub> production could be combined with hydrogen production, thereby also diversifying and adding value to the hydrogen industry.

## Author contributions

Dhananjai Pangotra: conceptualization, investigation, formal analysis, validation, writing – original draft. Lénárd-István Csepei: conceptualization, writing – review & editing. Arne Roth: conceptualization, supervision, writing – review & editing. Volker Sieber: supervision, writing – review & editing. Luciana Vieira: conceptualization, supervision, writing – review & editing.

## Conflicts of interest

There are no conflicts to declare.

## Acknowledgements

The authors thank Prof. Cordt Zollfrank (TUM-CS) for allowing access to SEM. Dr Tobias Graßl from Condias GmbH is deeply acknowledged for sharing scientific *know-how* on BDD electrodes. We thank Dr Leonardo Castañeda Losada for reading this manuscript and providing constructive feedback. All authors express their gratitude to the European Commission for the financial support of this research within the European Framework Programme for Research and Innovation Horizon 2020 (Grant No. 768789).

## References

- 1 Global Hydrogen Peroxide Market Outlook, <https://www.expertmarketresearch.com/reports/hydrogen-peroxide-market>, (accessed 20 August 2021, 2021).
- 2 A. Rubio-Clemente, E. Chica and G. Peñuela, *Environ. Sci. Pollut. Res.*, 2019, **26**, 4462–4473.
- 3 Chlorine or Hydrogen Peroxide – Which is Better for Treating Water?, <https://www.uswatersystems.com/blog/chlorine-or-hydrogen-peroxide>, (accessed 17 May 2022, 2021).
- 4 D. Horová, J. Nováková, L. Pelíšková, J. Kohout, J. Šafář, K. Hrachovcová and V. Tokarová, *React. Kinet., Mech. Catal.*, 2020, **130**, 1077–1092.
- 5 A. D. Ortiz-Marin, E. R. Bandala, K. Ramírez, G. Moeller-Chávez, L. Pérez-Estrada, B. Ramírez-Pereda and L. E. Amabilis-Sosa, *React. Kinet., Mech. Catal.*, 2022, **135**, 639–654.
- 6 R. Hage and A. Lienke, *Angew. Chem., Int. Ed.*, 2005, **45**, 206–222.



7 N. de la Fuente, L. Chen, J. A. Wang, J. González and J. Navarrete, *React. Kinet., Mech. Catal.*, 2021, **132**, 1119–1135.

8 H. Shuangyang, Hi Tech Chemical Co Ltd, A kind of deodorization of crude sulfate turpentine and the production method of sulfate turpentine, CN106281041B, 2016.

9 Institute of Chemical Industry of Forest Products of CAF, Refining method for desulphurizing and deodorizing crude sulphate turpentine, CN101654597B, 2009.

10 J. C. Rubio-Romero, M. D. C. Pardo-Ferreira, J. A. Torrecilla-Garcia and S. Calero-Castro, *Saf. Sci.*, 2020, **129**, 104830.

11 G. Lewandowski, M. Kujbida and A. Wróblewska, *React. Kinet., Mech. Catal.*, 2021, **132**, 983–1001.

12 L. Pierri, A. Gemenetzi, A. Mavrogiorgou, J. Borges Regitano, Y. Deligiannakis and M. Louloudi, *Mol. Catal.*, 2020, **489**, 110946.

13 J. D. Tibbetts, W. B. Cunningham, M. Vezzoli, P. Plucinski and S. D. Bull, *Green Chem.*, 2021, **23**, 5449–5455.

14 A. S. Gohardani, J. Stanojev, A. Demairé, K. Anflo, M. Persson, N. Wingborg and C. Nilsson, *Prog. Aerosp. Sci.*, 2014, **71**, 128–149.

15 M. Hävecker, S. Wrabetz, J. Kröhnert, L.-I. Csepei, R. Naumann d'Alnoncourt, Y. V. Kolen'ko, F. Girgsdies, R. Schlögl and A. Trunschke, *J. Catal.*, 2012, **285**, 48–60.

16 S. T. Renu Singh, M. Srivastava and A. Shukla, *Agric. Eng. Int.: CIGR J.*, 2014, **16**, 173–181.

17 J. Krischan, A. Makaruk and M. Harasek, *J. Hazard. Mater.*, 2012, **215–216**, 49–56.

18 R. L. Myers, *The 100 Most Important Chemical Compounds: A Reference Guide*, Greenwood Press, 2007.

19 L. Pesterfield, *J. Chem. Educ.*, 2009, **86**, 1182.

20 A. T. Murray, S. Voskian, M. Schreier, T. A. Hatton and Y. Surendranath, *Joule*, 2019, **3**, 2942–2954.

21 J. M. Campos-Martin, G. Blanco-Brieva and J. L. Fierro, *Angew. Chem., Int. Ed.*, 2006, **45**, 6962–6984.

22 S. C. Perry, D. Pangotra, L. Vieira, L.-I. Csepei, V. Sieber, L. Wang, C. Ponce de León and F. C. Walsh, *Nat. Rev. Chem.*, 2019, **3**, 442–458.

23 J. García-Serna, T. Moreno, P. Biasi, M. J. Cocero, J.-P. Mikkola and T. O. Salmi, *Green Chem.*, 2014, **16**, 2320–2343.

24 X. Shi, S. Back, T. M. Gill, S. Siahrostami and X. Zheng, *Chem.*, 2021, **7**, 38–63.

25 Evonik, Hydrogen Peroxide for Pulp and Paper Industry, <https://active-oxygens.evonik.com/product/h2o2/downloads/applications-hydrogen-peroxide-for-the-pulp-and-paper-industry-en.pdf>, (accessed 29 March 2022).

26 K. Wenderich, B. A. M. Nieuweweme, G. Mul and B. T. Mei, *ACS Sustainable Chem. Eng.*, 2021, **9**, 7803–7812.

27 C. Minke, M. Suermann, B. Bensmann and R. Hanke-Rauschenbach, *Int. J. Hydrogen Energy*, 2021, **46**, 23581–23590.

28 S. Kiemel, T. Smolinka, F. Lehner, J. Full, A. Sauer and R. Miehe, *Int. J. Energy Res.*, 2021, **45**, 9914–9935.

29 T. Kang, B. Li, Q. Hao, W. Gao, F. Bin, K. N. Hui, D. Fu and B. Dou, *ACS Sustainable Chem. Eng.*, 2020, **8**, 15005–15012.

30 S. Y. Park, H. Abroshan, X. Shi, H. S. Jung, S. Siahrostami and X. Zheng, *ACS Energy Lett.*, 2019, **4**, 352–357.

31 C. Zhang, R. Lu, C. Liu, L. Yuan, J. Wang, Y. Zhao and C. Yu, *Adv. Funct. Mater.*, 2021, **31**, 2100099.

32 X. Shi, S. Siahrostami, G. L. Li, Y. Zhang, P. Chakthranont, F. Studt, T. F. Jaramillo, X. Zheng and J. K. Norskov, *Nat. Commun.*, 2017, **8**, 701.

33 S. R. Kelly, X. Shi, S. Back, L. Vallez, S. Y. Park, S. Siahrostami, X. Zheng and J. K. Nørskov, *ACS Catal.*, 2019, **9**, 4593–4599.

34 T. Shiragami, H. Nakamura, J. Matsumoto, M. Yasuda, Y. Suzuri, H. Tachibana and H. Inoue, *J. Photochem. Photobiol. A*, 2015, **313**, 131–136.

35 F. Kuttassery, S. Mathew, S. Sagawa, S. N. Remello, A. Thomas, D. Yamamoto, S. Onuki, Y. Nabetani, H. Tachibana and H. Inoue, *ChemSusChem*, 2017, **10**, 1909–1915.

36 C. Xia, S. Back, S. Ringe, K. Jiang, F. Chen, X. Sun, S. Siahrostami, K. Chan and H. Wang, *Nat. Catal.*, 2020, **3**, 125–134.

37 S. Mavrikis, M. Göltz, S. Rosiwal, L. Wang and C. Ponce de León, *ACS Appl. Energy Mater.*, 2020, **3**, 3169–3173.

38 S. Mavrikis, M. Göltz, S. C. Perry, F. Bogdan, P. K. Leung, S. Rosiwal, L. Wang and C. Ponce de León, *ACS Energy Lett.*, 2021, **6**, 2369–2377.

39 K. Wenderich, B. A. M. Nieuweweme, G. Mul and B. T. Mei, *ACS Sustainable Chem. Eng.*, 2021, **9**, 7803–7812.

40 C. P. Chardon, T. Matthée, R. Neuber, M. Fryda and C. Comminellis, *ChemistrySelect*, 2017, **2**, 1037–1040.

41 S. Maljuric, W. Jud, C. O. Kappe and D. Cantillo, *J. Flow Chem.*, 2020, **10**, 181–190.

42 D. Pangotra, L.-I. Csepei, A. Roth, C. Ponce de León, V. Sieber and L. Vieira, *Appl. Catal., B*, 2022, **303**, 120848.

43 T. M. Gill, L. Vallez and X. Zheng, *ACS Energy Lett.*, 2021, **6**, 2854–2862.

44 B. J. Deadman, K. Hellgardt and K. K. Hii, *React. Chem. Eng.*, 2017, **2**, 462–466.

45 G. Eisenberg, *Ind. Eng. Chem., Anal. Ed.*, 1943, **15**, 327–328.

46 Z. Machala, B. Tarabova, K. Hensel, E. Spetlikova, L. Sikurova and P. Lukes, *Plasma Processes Polym.*, 2013, **10**, 649–659.

47 K. Fuku, Y. Miyase, Y. Miseki, T. Gunji and K. Sayama, *ChemistrySelect*, 2016, **1**, 5721–5726.

48 L. Fan, X. Bai, C. Xia, X. Zhang, X. Zhao, Y. Xia, Z.-Y. Wu, Y. Lu, Y. Liu and H. Wang, *Nat. Commun.*, 2022, **13**, 2668.

49 P. A. Michaud, M. Panizza, L. Ouattara, T. Diaco, G. Foti and C. Comminellis, *J. Appl. Electrochem.*, 2003, **33**, 151–154.

50 S. Palamutcu, in *Handbook of Life Cycle Assessment (LCA) of Textiles and Clothing*, ed. S. S. Muthu, Woodhead Publishing, 2015, pp. 31–61.

51 K. Wenderich, W. Kwak, A. Grimm, G. J. Kramer, G. Mul and B. Mei, *Sustainable Energy Fuels*, 2020, **4**, 3143–3156.

52 S. Chu, Y. Cui and N. Liu, *Nat. Mater.*, 2017, **16**, 16–22.

53 S. C. Perry, S. Mavrikis, L. Wang and C. Ponce de León, *Curr. Opin. Electrochem.*, 2021, **30**, 100792.

54 J. V. Macpherson, *Phys. Chem. Chem. Phys.*, 2015, **17**, 2935–2949.

